Found Phys (2015) 45:333–353
DOI 10.1007/s10701-015-9866-9

Discrete Excitation Spectrum of a Classical Harmonic Oscillator in Zero-Point Radiation

Wayne Cheng-Wei Huang · Herman Batelaan

Received: 29 May 2014 / Accepted: 9 January 2015 / Published online: 21 January 2015

Abstract We report that upon excitation by a single pulse, a classical harmonic oscillator immersed in the classical electromagnetic zero-point radiation exhibits a discrete harmonic spectrum in agreement with that of its quantum counterpart. This result is interesting in view of the fact that the vacuum field is needed in the classical calculation to obtain the agreement.

Keywords Stochastic electrodynamics · Quantum mechanics · Classical dynamics · Vacuum field · Harmonic oscillator · Excitation

1 Introduction

Historically, the discreteness of atomic spectra motivated the early development of quantum mechanics. Modern quantum mechanics describes atomic spectra with high accuracy. Classical mechanics incorrectly predicts the radiation death of an atom and no discrete states. In the theory of stochastic electrodynamics (SED) classical mechanics is modified by adding a classical vacuum field. The vacuum field is called classical as it is a solution to Maxwell's equations. The spectrum of this field is also required to exhibit Lorentz invariance [1,2]. Planck's constant $\hbar$ is brought into the classical vacuum field as an overall factor that sets the field strength. SED avoids radiation death in that the electron reaches an energy balance between radiative decay

W. C.-W. Huang
Department of Physics and Astronomy, Texas A&M University, College Station, TX 77843, USA
e-mail: u910134@alumni.nthu.edu.tw

H. Batelaan (✉)
Department of Physics and Astronomy, University of Nebraska-Lincoln, Lincoln, NE 68588, USA
e-mail: hbatelaan2@unl.edu

and vacuum field absorption. This leads to the existence of a ground state. However, the prediction of discrete atomic spectra including excited states appears not to be within reach of SED. Indeed, Peter W. Milonni has commented in his well-known book *The Quantum Vacuum* that "Being a purely classical theory of radiation and matter, SED is unable… to account for the discrete energy levels of the interacting atoms" [3].

Some authors, do not share this view and have recently claimed that SED accounts for the behavior associated with quantized states [4]. Even if these claims for SED were correct, one may be tempted to ignore SED as a viable alternative to quantum mechanics altogether. After all, experimental tests of Bell's inequalities establish that nature behaves in a nonlocal-real fashion, which appears to rule out any classical theory. The proponents of SED counter this idea by demonstrating entanglement-like properties [5]. In a broader view, SED is one of several attempts to build an "emergent quantum theory" [4].

In this paper we attempt to falsify SED with one counter example. We limit ourselves to the excitation process of an harmonic oscillator that is initially in the ground state. The results are compared to a fully quantum mechanical calculation. (Our original intent was to identify the limits of the validity range of SED before using it as an convenient means to study vacuum field effects on ground states). We find that SED can reproduce the discrete excitation spectrum of the harmonic oscillator, where the discreteness is explained as a result of parametric resonance (see detailed results and discussion below). This substantiates some claims by Cetto and gives credence to the idea that a full classical understanding of the Planck spectrum is possible [4] as it relies on the equidistant discrete spectrum of the harmonic oscillator. It is interesting and perhaps surprising that it is claimed that classical physics can explain physics phenomena that were long thought to be the exclusive domain of quantum mechanics. This list appears to include amongst others, the Black-Body Planck spectrum [4], the Casimir effect [6], and weak measurement [7].

We failed to provide a counter example to SED for the excitation spectrum of the harmonic oscillator. Nevertheless, the individual outcomes of measurements for SED may not agree with quantum mechanics. The quantum postulate for measurement states that individual outcomes for energy measurements can only take on energy eigenvalues, in agreement with observation. For the harmonic oscillator these outcomes are discrete, while the SED results in our study have a continuous distribution of energies for individual trajectories. It remains to be seen if SED can describe an individual measurement as the interaction between two systems (such as harmonic oscillators or atoms) that would mimic quantum mechanics and observation.

The organization of this paper is the following. First, the quantum and classical SED oscillator are considered. Their excitation spectra are obtained through numerically solving the equations of motion. A perturbative analysis is also given to provide insights to the underlying mechanism of the integer-spaced excitation spectrum of the classical SED oscillator.

2 Quantum Harmonic Oscillator

A semi-1D driven quantum harmonic oscillator can be constructed from an anisotropic 3D driven quantum harmonic oscillator. Treating the driving field as classical, the Hamiltonian for the 3D driven quantnum harmonic oscillator has the form [8]

$$\widehat{H}_{qm} = \frac{\left(\hat{\mathbf{p}} - q\mathbf{A}_p(\hat{\mathbf{r}}, t)\right)^2}{2m} + q\phi_p(\hat{\mathbf{r}}, t) + \frac{m\omega_x^2}{2}\hat{x}^2 + \frac{m\omega_y^2}{2}\hat{y}^2 + \frac{m\omega_z^2}{2}\hat{z}^2, \quad (1)$$

where $\hat{\mathbf{p}} = -i\hbar\nabla = (\hat{p}_x, \hat{p}_y, \hat{p}_z)$, $\hat{\mathbf{r}} = (\hat{x}, \hat{y}, \hat{z})$, m is the mass, q is the charge of the harmonic oscillator, and $(\phi_p, \mathbf{A}_p)$ is the driving field. The anisotropic harmonic oscillator has natural frequencies $\omega_x \equiv \omega_0$ and $\omega_y = \omega_z \equiv \omega_s$ for the harmonic potentials along the x, y, and z axes. The use of the Coulomb gauge ($\nabla \cdot \mathbf{A}_p = 0$) makes $\phi_p = 0$ in the absence of external charges and also $\hat{\mathbf{p}} \cdot \mathbf{A}_p = \mathbf{A}_p \cdot \hat{\mathbf{p}}$. Therefore, under the Coulomb gauge the Hamiltonian in Eq. (1) can be written as

$$\widehat{H}_{qm} = \left(\widehat{H}_x + \widehat{H}_y + \widehat{H}_z\right) + \widehat{H}', \quad (2)$$

where the unperturbed Hamiltonians are

$$\begin{aligned} \widehat{H}_x &\equiv \frac{\hat{p}_x^2}{2m} + \frac{m\omega_0^2}{2}\hat{x}^2, \\ \widehat{H}_y &\equiv \frac{\hat{p}_y^2}{2m} + \frac{m\omega_s^2}{2}\hat{y}^2, \\ \widehat{H}_z &\equiv \frac{\hat{p}_z^2}{2m} + \frac{m\omega_s^2}{2}\hat{z}^2, \end{aligned} \quad (3)$$

and the interaction Hamiltonian is

$$\widehat{H}' = -\frac{q}{2m}\left(2\mathbf{A}_p \cdot \hat{\mathbf{p}} - q\mathbf{A}_p^2\right). \quad (4)$$

In our study, a propagating Gaussian pulse is used as the driving field,

$$\mathbf{A}_p = A_p \cos\left(\mathbf{k}_p \cdot \hat{\mathbf{r}} - \omega_p\tau\right) \exp\left[-\left(\frac{\mathbf{k}_p \cdot \hat{\mathbf{r}}}{|\mathbf{k}_p|\Delta x} - \frac{\tau}{\Delta t}\right)^2\right]\boldsymbol{\varepsilon}_p, \quad (5)$$

where $\tau \equiv t - t_c$. The pulse center time t_c is the moment when the Gaussian pulse attains its maximum value at the origin. The temporal width of the pulse is Δt, and the spatial width is $\Delta x = c\Delta t$. The wave vector of the carrier wave is denoted as $\mathbf{k}_p = \omega_p/c\left(\sin\theta_p, 0, \cos\theta_p\right)$, and the field polarization is $\boldsymbol{\varepsilon}_p = \left(\cos\theta_p, 0, -\sin\theta_p\right)$. In the simulation, the field amplitude is chosen to be $A_p = 1.5 \times 10^{-9}$ Vs/m, and the polarization angle is $\theta_p = \pi/4$. While the unperturbed Hamiltonian in Eq. (3) defines a unperturbed basis states for the oscillator, the interaction Hamiltonian in Eq. (4) can induce transitions between these basis states. The energy levels of the oscillator are

$$E_{nmk} = E_n + E_m + E_k, \tag{6}$$

where $E_n = \hbar\omega_0(n + 1/2)$, $E_m = \hbar\omega_s(m + 1/2)$, and $E_k = \hbar\omega_s(k + 1/2)$ are the eigenvalues to the unperturbed Hamiltonians. A transition between the state $|nmk\rangle$ and the state $|abc\rangle$ occurs when $|E_{abc} - E_{nmk}| = j\hbar\omega_p$. Here the parameter j signifies a j-th order process. Assuming $\omega_s \gg \omega_0$ and $w_p \simeq \omega_0$, a high-order processes ($j \gg 1$) is required to drive any $\Delta m > 0$ or $\Delta k > 0$ transitions. Given the parameters in our simulation, only the lowest excited states $|n00\rangle$ with eigen-energies $E_{n00} = E_n + \hbar\omega_s$ will be considered. Therefore, the 3D anisotropic harmonic oscillator can be seen as a semi-1D oscillator in the x-direction, constrained by the strong potentials in the y- and z-direction.

As only $|n00\rangle$ states will be considered, we let $\hat{\mathbf{p}} = \hat{p}_x\boldsymbol{\varepsilon}_x$ and $\hat{\mathbf{r}} = \hat{x}\boldsymbol{\varepsilon}_x$, in the Hamiltonian to simplify the notation. The unit vector $\boldsymbol{\varepsilon}_x$ is along the x-direction, $\boldsymbol{\varepsilon}_x = (1, 0, 0)$. The oscillator is initially in the ground state. After excitation the state $|\psi\rangle$(t) becomes a superposition of N eigenstates $|n00\rangle$,

$$|\psi\rangle(t) = \sum_{n=1}^{N} c_n|n00\rangle e^{-i\omega_n t}e^{-i\omega_s t}, \tag{7}$$

where $\omega_n = \omega_0(n + 1/2)$. To obtain the coefficients of the excited state $|\psi\rangle$(t), we solve the Schrödinger equation,

$$\frac{d}{dt}C(t) = -\frac{i}{\hbar}H^{'}C(t), \tag{8}$$

where $C(t)$ is a $N \times 1$ matrix and $H^{'}$ is a $N \times N$ matrix,

$$C = \begin{pmatrix} c_1(t) \\ c_2(t) \\ \vdots \\ c_N(t) \end{pmatrix}, \quad H^{'} = \begin{pmatrix} \cdots \\ \vdots\ H^{'}_{nm}e^{i\omega_{nm}t}\ \vdots \\ \cdots \end{pmatrix}. \tag{9}$$

For each element in the matrix $H^{'}$, $H^{'}_{nm} = \langle n00|\widehat{H}^{'}|m00\rangle$ and $\omega_{nm} \equiv \omega_n - \omega_m$. The total number of energy levels is chosen to be $N = 20$ for the given parameters, so that the population of the highest energy state is zero. Since resonances at higher-harmonics depend critically on the spatial nonlinearity of the pulse field, the dipole approximation is not sufficient for the study of the excitation spectrum, making a numerical approach to this problem convenient. In the simulation, the spatial dependence of the pulse field $\mathbf{A}_p$ is multipole-expanded up to the $20th$-order to reach numerical convergence. Lastly, the matrix element of the operators $\hat{x}$ and $\hat{p}_x$ are specified by

$$\langle n00|\hat{x}|m00\rangle = \sqrt{\frac{\hbar}{2m\omega_0}}\left(\sqrt{n}\delta_{m,n-1} + \sqrt{n+1}\delta_{m,n+1}\right)$$

$$\langle n00|\hat{p}_x|m00\rangle = i\sqrt{\frac{\hbar m\omega_0}{2}}\left(\sqrt{n}\delta_{m,n-1} - \sqrt{n+1}\delta_{m,n+1}\right). \tag{10}$$

Finally, we note that time-dependent perturbation quantum theory gives results in agreement with the above simulation (see Appendix 2).

3 Classical Harmonic Oscillator in the Vacuum Field

In the classical case, a similar construction can be done to construct a semi-1D driven classical harmonic oscillator. To account for the vacuum field and the radiation reaction, the additional field Hamiltonian $H_F = \frac{\epsilon_0}{2}\int d^3\mathbf{r}\left(|\mathbf{E}_p+\mathbf{E}_{vac}|^2+c^2\,|\mathbf{B}_p+\mathbf{B}_{vac}|^2\right)$ needs to be included. Having a semi-1D harmonic oscillator immersed in the vacuum field, the classical Hamiltonian is

$$H_{cl} = \left(\frac{p_x^2}{2m} + \frac{m\omega_0^2}{2}x^2\right) - \frac{q}{2m}\left(2\mathbf{A}\cdot\mathbf{p} - q\mathbf{A}^2\right) + H_F, \tag{11}$$

where $\mathbf{A} = \mathbf{A}_p + \mathbf{A}_{vac}$, $\mathbf{p} = p_x\boldsymbol{\varepsilon}_x$, and $\mathbf{r} = x\boldsymbol{\varepsilon}_x$. The vacuum field is specified by

$$\mathbf{A}_{vac} = \sum_{\mathbf{k},\lambda}\sqrt{\frac{\hbar}{\epsilon_0 V\omega}}\cos\left(\mathbf{k}\cdot\mathbf{r} - \omega t + \tilde{\theta}_{\mathbf{k},\lambda}\right)\boldsymbol{\varepsilon}_{\mathbf{k},\lambda}, \tag{12}$$

where $\omega = c|\mathbf{k}|$, $\tilde{\theta}_{\mathbf{k},\lambda}$ is the random phase uniformly distributed in $[0, 2\pi]$, and V is the physical volume occupied by the vacuum field. The two unit vectors, $\boldsymbol{\varepsilon}_{\mathbf{k},1}$ and $\boldsymbol{\varepsilon}_{\mathbf{k},2}$, describe a mutually orthogonal polarization basis in a plane perpendicular to the wave vector $\mathbf{k}$. The pulse field $\mathbf{A}_p$ is identical to that in Eq. (5) except for $\mathbf{r}$ being a classical quantity rather than an operator,

$$\mathbf{A}_p = A_p\cos\left(\mathbf{k}_p\cdot\mathbf{r} - \omega_p\tau\right)\exp\left[-\left(\frac{\mathbf{k}_p\cdot\mathbf{r}}{|\mathbf{k}_p|\Delta x} - \frac{\tau}{\Delta t}\right)^2\right]\boldsymbol{\varepsilon}_p. \tag{13}$$

From the Hamiltonian, the classical equation of motion follows,

$$m\ddot{x} = -m\omega_0^2 x + m\Gamma\dddot{x} + q\left[\left(E_p^{(x)} + E_{vac}^{(x)}\right) + \left(\mathbf{v}\times(\mathbf{B}_p + \mathbf{B}_{vac})\right)^{(x)}\right], \tag{14}$$

where $\Gamma \equiv \frac{2q^2}{3mc^3}\frac{1}{4\pi\epsilon_0}$ and $m\Gamma\dddot{x}$ represents the radiation reaction field [9,10]. Under the Coulomb gauge, the electric field is given by $\mathbf{E} = -\frac{\partial\mathbf{A}}{\partial t}$ and the magnetic field by $\mathbf{B} = \nabla\times\mathbf{A}$. The symbol $E^{(x)}$ denotes the x-component of the vector $\mathbf{E}$. Because $\mathbf{v} = \boldsymbol{\varepsilon}_x p_x/m$, the magnetic part of the Lorentz force is zero. To avoid numerical runaway solutions, we assume the point-particle description of the charged particle and make the usual approximation $m\Gamma\dddot{x} \simeq -m\Gamma\omega_0^2\dot{x}$ for numerical simulation [11,12].

Thus, the equation of motion used for simulation is

$$m\ddot{x} \simeq -m\omega_0^2 x - m\Gamma\omega_0^2\dot{x} + q\left[\left(E_p^{(x)} + E_{vac}^{(x)}\right) + \left(\mathbf{v}\times(\mathbf{B}_p + \mathbf{B}_{vac})\right)^{(x)}\right]. \quad (15)$$

Note that we ignore nonlinear backaction of the field on the dynamics of the charged particle.

To carry out the simulation, an isotropic sampling of N_ω vacuum field modes $(\mathbf{k}_i, \lambda)$ is needed [13]. The wave vectors $\mathbf{k}_i$ are chosen to have frequencies within the finite range $[\omega_0 - \Delta/2, \omega_0 + \Delta/2]$, where Δ is the vacuum field frequency bandwidth and it is chosen to be $\Delta = 2.2\times 10^2\Gamma\omega_0^2$, much larger than the oscillator's resonance bandwidth $\Gamma\omega_0^2$. The vacuum field modes in $\mathbf{k}$-space are sampled in spherical coordinates. In the following, we give the specific steps of the sampling method. For $i = 1\ldots N_\omega$, the wave vector are sampled by

$$\mathbf{k}_i = \begin{pmatrix} k_i\sin\theta_i\cos\phi_i \\ k_i\sin\theta_i\sin\phi_i \\ k_i\cos\theta_i \end{pmatrix}, \quad (16)$$

where

$$\begin{cases} k_i = (3\kappa_i)^{1/3} \\ \theta_i = \cos^{-1}(\vartheta_i) \\ \phi_i = \varphi_i, \end{cases} \quad (17)$$

and

$$\begin{cases} \kappa_i = (\omega_0 - \Delta/2)^3/3c^3 + (i-1)\Delta\kappa \\ \vartheta_i = R_i^{(1)} \\ \varphi_i = R_i^{(2)}. \end{cases} \quad (18)$$

The random number $R^{(1)}$ is uniformly distributed in $[-1, 1]$, and $R^{(2)}$ is uniformly distributed in $[0, 2\pi]$. The stepsize $\Delta\kappa$ is specified by $\Delta\kappa = \left[(\omega_0 + \Delta/2)^3 - (\omega_0 - \Delta/2)^3\right]/\left[3c^3(N_\omega - 1)\right]$. Finally, the polarization vectors are sampled by

$$\boldsymbol{\varepsilon}_{\mathbf{k},1} = \begin{pmatrix} \cos\theta_i\cos\phi_i\cos\chi_i - \sin\phi_i\sin\chi_i \\ \cos\theta_i\sin\phi_i\cos\chi_i + \cos\phi_i\sin\chi_i \\ -\sin\theta_i\cos\chi_i \end{pmatrix},$$
$$\boldsymbol{\varepsilon}_{\mathbf{k},2} = \begin{pmatrix} -\cos\theta_i\cos\phi_i\sin\chi_i - \sin\phi_i\cos\chi_i \\ -\cos\theta_i\sin\phi_i\sin\chi_i + \cos\phi_i\cos\chi_i \\ \sin\theta_i\sin\chi_i \end{pmatrix}. \quad (19)$$

Such a sampling method is computationally more efficient in reaching numerical convergence, and it approaches cartesian sampling as $N_\omega \to \infty$ (see Fig. 1). The volume factor V in the vacuum field strength $\sqrt{\frac{\hbar}{\epsilon_0 V\omega}}$ can be estimated by $V \simeq (2\pi)^3 N_\omega/V_{\mathbf{k}}$.

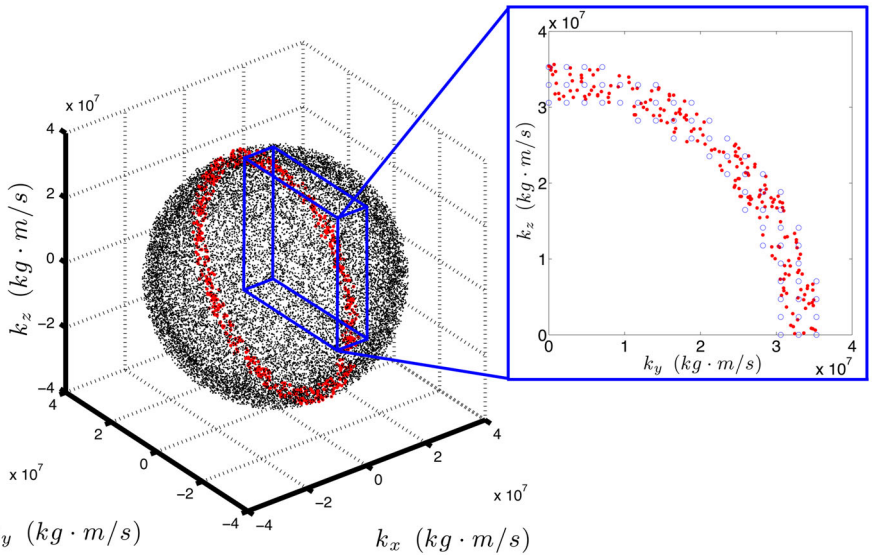

Fig. 1 The sampled vacuum field modes in **k**-space. *Left* the sampled vacuum field modes (*black dots*) are distributed in a spherical shell with thickness Δ/c. The number of sampled modes shown here is $N_\omega = 20,000$. A slice of the spherical shell at $\mathbf{k}_x \simeq 0$ is highlighted (*red dots*). *Right* a quarter of the highlighted slice (*red dots*) is projected on the $k_y k_z$-plane. The modes sampled with cartesian sampling (*blue circles*) are shown for comparison (Color figure online)

Here, the **k**-space volume $V_\mathbf{k} = 4\pi/3c^3\Big[(\omega_0 + \Delta/2)^3 - (\omega_0 - \Delta/2)^3\Big]$ encloses the sampled vacuum field modes $\mathbf{k}_i$ in the spherical shell $\Big[(\omega_0 - \Delta/2)/c, (\omega_0 + \Delta/2)/c\Big]$.

The general statistics of the vacuum field such as correlation functions have been studied in detail [2]. Our mode sampling method discussed here has proven to be valid and simulate the vacuum field properly, leading to the correct Gaussian statistics of the oscillator [2]. More details about the mode sampling method and the oscillator statistics are provided in [13].

4 Results and Mechanism

We give the simulation result for the excitation spectrum in Fig. 2. The horizontal axis is the pulse frequency ω_p which is scanned across to the first, second, and third harmonics of the fundamental frequency ω_0. The vertical axis shows the quantum expectation value for the quantum mechanical calculation, and the classical ensemble average of the excited energy for the classical calculation. A superficial reading of the spectrum in Fig. 2 might equate its three peaks with the first, second, and third excited states of the harmonic oscillator, effectively reading them off as energy levels. This is not the case in either the classical or the quantum calculations. In the classical calculation, it is not the case because there are no such elements as "states" in the theory. In the quantum calculation, it is not the case because each resonance peak has

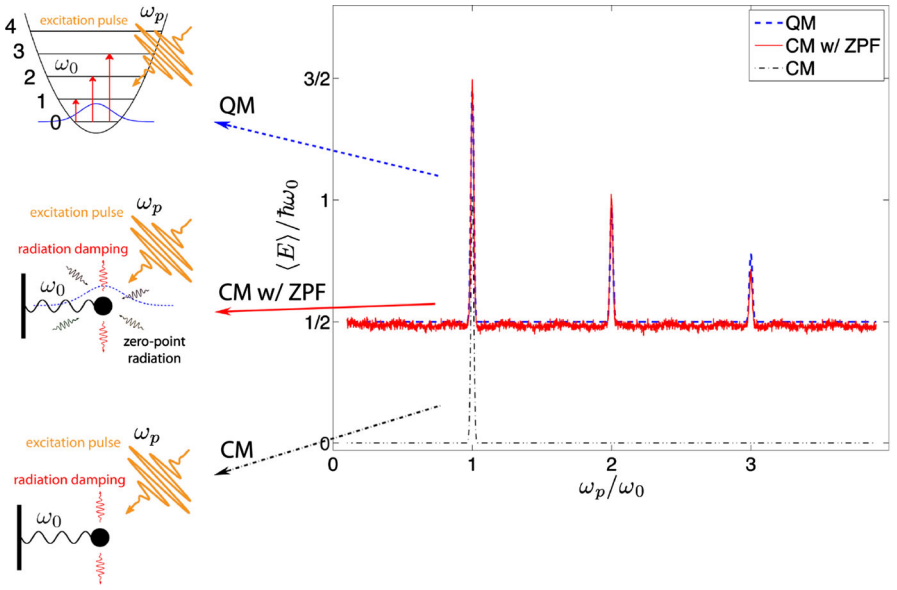

Fig. 2 The excitation spectra of harmonic oscillators in different theories. *Left* Schematics of harmonic oscillators are shown for quantum theory (*left-top*), for classical theory as modified by the vacuum field, or the zero-point field (ZPF) (*left-middle*), and for the standard classical theory (*left-bottom*). The *red arrows* in the quantum system represents the one-step transition at different pulse frequencies ω_p. When $\omega_p = \omega_0$, the transition is only between the neighboring states, namely $0 \to 1$, $1 \to 2$, and so on. When $\omega_p = 2\omega_0$, the transition is only between every other neighboring states, namely $0 \to 2$, $2 \to 4$, and so on. Same argument applies to $\omega_p = 3\omega_0$. *Right* the averaged value of energy $\langle E \rangle$ after excitation is plotted as a function of pulse frequency ω_p. For the classical theory, the ensemble average is computed. For the quantum theory, the expectation value is computed. The classical oscillator in the vacuum field (*red solid line*) exhibits an excitation spectrum in agreement with the quantum result (*blue broken line*). The number of vacuum field modes used in this simulation is $N_\omega = 500$. In the absence of the vacuum field, the classical oscillator has only one single resonance peak at the natural frequency ω_0 (*black dotted line*). The excitation peak heights and the relative ratio are confirmed by the classical perturbation analysis (Color figure online)

contributions from the populations of all energy levels, $\langle E \rangle = \sum_n |c_n|^2 \hbar\omega_0 (n + 1/2)$. In other words, both one-step and multi-step transitions occur at each resonance peak.

When the vacuum field is absent, the classical harmonic oscillator has only a single resonance at its natural frequency. With the vacuum field acting as a background perturbation, the classical harmonic oscillator exhibits an integer-spaced excitation spectrum, or if one likes, a "quantized" excitation spectrum. The position and the magnitude of the resonance peaks are in agreement with the quantum mechanical result. Such an agreement between the classical theory (as modified by the vacuum field) and quantum mechanics appears to be astonishing, given that the theory is fully classical and no quantization condition is added.

In the simulation, we can turn on and off the nonlinearity of either the vacuum field or the pulse field. The excitation spectrum was unaffected when only the nonlinearity of the vacuum field is turned off. The excitation at the higher-harmonics completely disappear when only the nonlinearity of the pulse field is turned off. Moreover, the magnitude of the excitation peak at ω_0 is also affected. This shows that the occurrence

of the integer-spaced excitation spectrum is solely due to the nonlinearity of the pulse field. To investigate the role of the vacuum field, we first consider a classical harmonic oscillator subject to only the pulse field,

$$m\ddot{x} = -m\omega_0^2 x + qE_p(x,t), \tag{20}$$

where $E_p(x,t) = E_0 \sin(k_p x - \omega_p \tau) \exp\left(-\tau^2/\Delta t^2\right)$, $\tau \equiv t - t_c$, $E_0 = -A_p \omega_p \cos(\theta_p)$, and $k_p = \omega_p/c \sin(\theta_p)$. Notice that the equation of motion discussed here, Eq. (20), is an approximation (the vacuum field is ignored for the evolution) to the equation of motion used in the simulation, Eq. (15). The reason why this approximation is made will now be explained. The simulation of Eq. (15) started at $t = 0$ with initial conditions $x = 0$ and $v = 0$. After a period of time longer than the relaxation time, $\tau_{rel} = 1/\Gamma\omega_0^2$, the memory of the initial condition is lost. As the driving from the vacuum field balances with the radiation damping, the harmonic oscillator reaches a steady state, and its position and velocity distributions are Gaussian due to statistical properties of the vacuum field [2,13]. We take from these Gaussian distributions the new initial conditions, x_0 and v_0, for our simplified evolution equation Eq. (20) and label the new initial time t_i ($\gg \tau_{rel}$). The excitation pulse E_p occurs later at time t_c, while the time for the simulation result to be recorded is still somewhat later at t_p. Therefore, the simplified equation of motion is thought to be valid from t_i to t_p, and the time interval $t_p - t_i$ should be much smaller than the damping time τ_{rel} (or the time it takes the vacuum field to change the particle's motion significantly). In the following, the time coordinate for Eq. (20) is offset by t_i, and x_0 and v_0 are taken as the initial conditions for solving Eq. (20).

The investigation of the excitation mechanism begins with Taylor expanding the spatial dependence of the pulse around $k_p x = 0$,

$$E_p(x,t) \simeq E_{1\omega_0}(x,t) + E_{2\omega_0}(x,t) + E_{3\omega_0}(x,t), \tag{21}$$

where

$$\begin{aligned} E_{1\omega_0}(x,t) &= -E_0 \sin(\omega_p \tau) \exp(-\tau^2/\Delta t^2), \\ E_{2\omega_0}(x,t) &= (k_p x) E_0 \cos(\omega_p \tau) \exp(-\tau^2/\Delta t^2), \\ E_{3\omega_0}(x,t) &= \left(\frac{k_p^2 x^2}{2}\right) E_0 \sin(\omega_p \tau) \exp(-\tau^2/\Delta t^2). \end{aligned} \tag{22}$$

To show that the three interaction terms in Eq. (22) correspond to excitation at the drive frequencies $1\omega_0$, $2\omega_0$, and $3\omega_0$, three equations of motion are solved in the following with individual interaction terms as the driving field. The equation for $1\omega_0$-excitation is given by,

$$\begin{aligned} m\ddot{x}_{1\omega_0} &= -m\omega_0^2 x_{1\omega_0} + qE_{1\omega_0}(x,t) \\ &= -m\omega_0^2 x_{1\omega_0} - qE_0 \sin(\omega_p \tau) \exp(-\tau^2/\Delta t^2). \end{aligned} \tag{23}$$

The full solution to this equation can be found as [14]

$$x_{1\omega_0} = x_{1c} + x_{1p}, \tag{24}$$

with

$$\begin{aligned} x_{1c}(t) &= D_0 \cos(\omega_0 t + \varphi_0), \\ x_{1p}(t) &= -\int_0^\infty d\omega f_1(\omega) \sin(\omega\tau), \end{aligned} \tag{25}$$

where

$$\begin{aligned} f_1(\omega) &\equiv \frac{\Delta t}{2\sqrt{\pi}} \frac{qE_0}{m(\omega_0^2 - \omega^2)} \exp\left[-\left(\frac{\omega - \omega_p}{2/\Delta t} \right)^2 \right], \\ D_0 &= \sqrt{(x_0 - x_{1p}(0))^2 + (v_0 - v_{1p}(0))^2/\omega_0^2}, \\ \cos(\varphi_0) &= (x_0 - x_{1p}(0))/D_0, \\ \sin(\varphi_0) &= -(v_0 - v_{1p}(0))/D_0\omega_0. \end{aligned} \tag{26}$$

Note that the complimentary solution x_{1c} depends on the initial conditions x_0 and v_0, but the particular solution x_{1p} does not. The particular solution of velocity is defined as $v_{1p} \equiv dx_{1p}/dt$. Here we assume the classical harmonic oscillator has the initial position x_0 and velocity v_0. The equation for $2\omega_0$-excitation is given by

$$\begin{aligned} m\ddot{x}_{2\omega_0} &= -m\omega_0^2 x_{2\omega_0} + qE_{2\omega_0}(x,t) \\ &= -m\omega_0^2 x_{2\omega_0} + q(k_p x_{2\omega_0}) E_0 \cos(\omega_p \tau) \exp(-\tau^2/\Delta t^2). \end{aligned} \tag{27}$$

This equation is solved with a perturbation method up to the first-order in $\varepsilon \equiv qE_0\lambda_0/mc^2$. Namely, substituting the perturbative expansion of the solution

$$x_{2\omega_0} \simeq x_{2c}^{(0)} + \varepsilon \left(x_{2c}^{(1)} + x_{2p}^{(1)} \right), \tag{28}$$

to Eq. (27), the perturbative terms can be solved iteratively,

$$\begin{aligned} x_{2c}^{(0)}(t) &= A_0 \cos(\omega_0 t + \phi_0), \\ x_{2c}^{(1)}(t) &= B_0 \cos(\omega_0 t + \xi_0), \\ x_{2p}^{(1)}(t) &= \left(\frac{k_p A_0}{2\varepsilon} \right) \int_0^\infty d\omega f_2(\omega) \cos(\omega\tau - \omega_0 t_c - \phi_0), \end{aligned} \tag{29}$$

where

$$f_2(\omega) \equiv \frac{\Delta t}{2\sqrt{\pi}} \frac{qE_0}{m(\omega_0^2 - \omega^2)} \exp\left[-\left(\frac{\omega - (\omega_p - \omega_0)}{2/\Delta t} \right)^2 \right],$$

$$
\begin{aligned}
&A_0 = \sqrt{x_0^2 + v_0^2/\omega_0^2},\\
&\cos(\phi_0) = x_0/A_0,\\
&\sin(\phi_0) = -v_0/A_0\omega_0,\\
&B_0 = \sqrt{\left(x_{2p}^{(1)}(0)\right)^2 + \left(v_{2p}^{(1)}(0)/\omega_0\right)^2},\\
&\cos(\xi_0) = -x_{2p}^{(1)}(0)/B_0,\\
&\sin(\xi_0) = v_{2p}^{(1)}(0)/B_0\omega_0.
\end{aligned}
\tag{30}
$$

The particular solution of velocity is defined as $v_{2p}^{(1)} \equiv dx_{2p}^{(1)}/dt$. Again, x_0 and v_0 are the initial conditions as defined previously. The equation for $3\omega_0$-excitation is given by

$$
\begin{aligned}
m\ddot{x}_{3\omega_0} &= -m\omega_0^2 x_{3\omega_0} + qE_{3\omega_0}(x,t)\\
&= -m\omega_0^2 x_{3\omega_0} + q\left(\frac{k_p^2 x_{3\omega_0}^2}{2}\right) E_0 \sin(\omega_p\tau)\exp(-\tau^2/\Delta t^2).
\end{aligned}
\tag{31}
$$

This equation is solved with a perturbation method up to the first-order in $\eta \equiv qE_0A_0/mc^2$. Namely, substituting the perturbative expansion of the solution

$$
x_{3\omega_0} \simeq x_{3c}^{(0)} + \eta\left(x_{3c}^{(1)} + x_{3p}^{(1)}\right),
\tag{32}
$$

to Eq. (31), the perturbative terms can be solved iteratively,

$$
\begin{aligned}
&x_{3c}^{(0)}(t) = A_0\cos(\omega_0 t + \phi_0),\\
&x_{3c}^{(1)}(t) = C_0\cos(\omega_0 t + \zeta_0),\\
&x_{3p}^{(1)}(t) = \left(\frac{k_p^2 A_0^2}{8\eta}\right)\int_0^\infty d\omega f_3(\omega)\sin(\omega\tau - 2\omega_0 t_c - 2\phi_0),
\end{aligned}
\tag{33}
$$

where,

$$
\begin{aligned}
&f_3(\omega) = \frac{\Delta t}{2\sqrt{\pi}}\frac{qE_0}{m(\omega_0^2-\omega^2)}\exp\left[-\left(\frac{\omega-(\omega_p-2\omega_0)}{2/\Delta t}\right)^2\right],\\
&A_0 = \sqrt{x_0^2 + v_0^2/\omega_0^2},\\
&\cos(\phi_0) = x_0/A_0,\\
&\sin(\phi_0) = -v_0/A_0\omega_0,\\
&C_0 = \sqrt{(x_{3p}^{(1)}(0))^2 + (v_{3p}^{(1)}(0)/\omega_0)^2},\\
&\cos(\zeta_0) = -x_{3p}^{(1)}(0)/C_0,\\
&\sin(\zeta_0) = v_{3p}^{(1)}(0)/C_0\omega_0.
\end{aligned}
\tag{34}
$$

The particular solution of velocity is defined as $v_{3p}^{(1)} \equiv dx_{3p}^{(1)}/dt$. The total energy change of the harmonic oscillators as described in Eqs. (23), (27), and (31) can be calculated through

$$W_\omega = \int_{-\infty}^{+\infty} qE_\omega(x_\omega, t)v_\omega(t)\,dt, \tag{35}$$

where the label ω is to be replaced by $1\omega_0$, $2\omega_0$, or $3\omega_0$. Using the solutions given above, the energy changes can be obtained for $\omega_p \simeq 1\omega_0$, $2\omega_0$, and $3\omega_0$ respectively,

$$\begin{aligned}
W_{1\omega_0} &= \frac{\sqrt{\pi}}{2}(D_0\omega_0)(qE_0\Delta t)\exp\left[-\left(\frac{\omega_p-\omega_0}{2/\Delta t}\right)^2\right]\cos(\omega_0 t_c+\varphi_0),\\
W_{2\omega_0} &= -\frac{\sqrt{\pi}}{4}(k_pA_0)(A_0\omega_0)(qE_0\Delta t)\exp\left[-\left(\frac{\omega_p-2\omega_0}{2/\Delta t}\right)^2\right]\Big[\sin(2\omega_0 t_c+2\phi_0)\\
&\quad +2\frac{\varepsilon B_0}{A_0}\sin(2\omega_0 t_c+\xi_0+\phi_0)\Big],\\
W_{3\omega_0} &= -\frac{\sqrt{\pi}}{8}\left(\frac{k_p^2A_0^2}{2}\right)(A_0\omega_0)(qE_0\Delta t)\exp\left[-\left(\frac{\omega_p-3\omega_0}{2/\Delta t}\right)^2\right]\Big[\cos(3\omega_0 t_c+3\phi_0)\\
&\quad +3\frac{\eta C_0}{A_0}\cos(3\omega_0 t_c+2\phi_0+\zeta_0)\Big].
\end{aligned} \tag{36}$$

As a result, the excitation at $\omega_p \simeq 1\omega_0$ is due to the harmonic resonance, while excitation at $\omega_p \simeq 2\omega_0$ and $\omega_p \simeq 3\omega_0$ is due to the parametric resonance [15,16]. The ensemble average of the energy changes in Eq. (36) can be evaluated using the statistical moments of the initial conditions (see Appendix 1 for details). As discussed earlier, the initial conditions are determined by the stationary state of the harmonic oscillator in the vacuum field. For evaluating $\langle W_{1\omega_0}\rangle$, $\langle x_0\rangle$ and $\langle v_0\rangle$ are used; for evaluating $\langle W_{2\omega_0}\rangle$, $\langle x_0^2\rangle$, $\langle v_0^2\rangle$, and $\langle x_0v_0\rangle$ are used; for evaluating $\langle W_{3\omega_0}\rangle$, $\langle x_0^4\rangle$, $\langle v_0^4\rangle$, $\langle x_0^2v_0^2\rangle$, $\langle x_0^3v_0\rangle$, and $\langle x_0v_0^3\rangle$ are used. Using the statistical moments given by Boyer's analysis [2], we obtain

$$\begin{aligned}
\langle W_{1\omega_0}\rangle &= \frac{\pi}{8}\frac{(qE_0\Delta t)^2}{m}\exp\left[-2\left(\frac{\omega_p-\omega_0}{2/\Delta t}\right)^2\right],\\
\langle W_{2\omega_0}\rangle &= \frac{\pi}{16}\frac{(qE_0\Delta t)^2}{m}\left(\frac{\hbar\omega_p}{mc^2}\right)\left(\frac{\omega_p}{\omega_0}\right)\sin^2(\theta_p)\exp\left[-2\left(\frac{\omega_p-2\omega_0}{2/\Delta t}\right)^2\right],\\
\langle W_{3\omega_0}\rangle &= \frac{3\pi}{16^2}\frac{(qE_0\Delta t)^2}{m}\left[\left(\frac{\hbar\omega_p}{mc^2}\right)\left(\frac{\omega_p}{\omega_0}\right)\sin^2(\theta_p)\right]^2\exp\left[-2\left(\frac{\omega_p-3\omega_0}{2/\Delta t}\right)^2\right],
\end{aligned} \tag{37}$$

where the relation between the electric field and the vector potential is given by $E_0 = -A_p\omega_p\cos(\theta_p)$. To illustrate the method of the ensemble averaging shown here, a detailed analysis of deriving $\langle W_{1\omega_0}\rangle$ is given in Appendix 1. With the parameters used in our simulation, namely the natural frequency $\omega_0 = 10^{16}$ rad/s, particle charge

$q = 1.60\times10^{-19}$ C, particle mass[1] $m = 9.11\times10^{-35}$ kg, polarization angle $\theta_p = \pi/4$, pulse duration $\Delta t = 10^{-14}$ s, pulse center time $t_c = 5\tau_{rel} = 1.60\times10^{-12}$ s, and field amplitude $A_p = 1.5\times10^{-9}$ Vs/m, the perturbation result shown in Eq. (37) gives the peak heights at $1\omega_0$, $2\omega_0$, and $3\omega_0$ as

$$\begin{aligned}\langle W_{1\omega_0}\rangle &\simeq 1.2\hbar\omega_0,\\ \langle W_{2\omega_0}\rangle &\simeq 0.6\hbar\omega_0,\\ \langle W_{3\omega_0}\rangle &\simeq 0.3\hbar\omega_0.\end{aligned} \tag{38}$$

The full spectrum can also be evaluated using Eq. (37), and the agreement with the simulation result (Fig. 2) is about 80 %. Therefore, the above perturbation analysis confirms that the occurrence of integer-spaced overtones is due to the parametric resonance through the nonlinearity of the pulse field. Before the arrival of the pulse, the vacuum field prepares the particle ensemble with a particular distribution in phase space. Such a distribution eventually determines the relative height for the excitation peaks.

In summary, while the quantized excitation spectrum of a quantum harmonic oscillator is explained by the intrinsic quantized energy levels and the transitions associated with nonlinear operators $\hat{x}^n$ in the excitation pulse, the "quantized" excitation of the classical harmonic oscillator is a result of parametric excitation due to the pulse and the initial conditions introduced by the vacuum field. In both theories, the integer-spaced overtones are caused by the nonlinearity of the pulse.

5 Discussion and Conclusions

We have shown that the classical harmonic oscillator in the vacuum field exhibits the same integer-spaced excitation spectrum as its quantum counterpart. This supports some of Cetto's claims [4], and is especially interesting given the classical SED explanation that based on these claims can be provided for the black body spectrum. Our simulation is limited in the sense that it cannot resolve resonances at fractional frequencies (such as $1/2\omega_0$ and $1/3\omega_0$). Such resonances are predicted by the quantum mechanical calculation, but are so weak that they are beyond the resolution of the SED simulation.

In this study, the classical and the quantum excitation spectrum are compared in terms of ensemble averages. The individual outcomes of measurements for SED appear not to agree with quantum mechanics. The quantum postulate for measurement states that individual outcomes for energy measurements can only take on energy eigenvalues, in agreement with observation. For the quantum harmonic oscillator these outcomes are discrete, while the classical theory of SED in our study gives a continuous distribution of energy outcomes for individual trajectories.

A question remains what a measurement constitutes in SED. If one would measure the frequency of the decay radiation, SED would likely predict this to be peaked

[1] The mass value is chosen to keep the integration time manageable without losing the physical characteristics of the problem.

around the natural frequency of the harmonic oscillator. It remains to be seen if the vacuum field can provide a mechanism to stimulate emission frequencies at the higher harmonics. Given that an excitation pulse can provide such a mechanism, it may be that the vacuum field will give rise to a similar decay spectrum to what quantum mechanics predicts. However, even if the SED decay spectrum would match the quantum mechanical spectrum, the amount of energy released in the decay will not match that of individual photons. The reason is that the radiated energy equals the amount of energy lost from the particle, which reflects its classical continuous spectrum.

Thus, in agreement with the nature of, and expanding on Milonni's comment; although SED can account for at least one discrete energy spectrum in terms of averaged energies, it does (up to this point) not match quantum mechanics. It would be interesting to investigate if the SED description of two interacting systems would modify these results in bring them closer to the quantum mechanical predictions.

Acknowledgments We gratefully acknowledge comments from Prof. Peter W. Milonni. The funding support comes from NSF Grant No. 0969506. This work was completed utilizing the Holland Computing Center of the University of Nebraska and the Extreme Science and Engineering Discovery Environment (XSEDE), which is supported by NSF Grant No. OCI-1053575.

6 The Derivation of $\langle W_{1\omega_0} \rangle$

In this appendix, the value of $\langle W_{1\omega_0} \rangle$ is calculated. This expounds the steps leading from Eq. (36) to Eq. (37). We will focus here on $\langle W_{1\omega_0} \rangle$ and indicate how the steps are different in notation for $\langle W_{2\omega_0} \rangle$ and $\langle W_{3\omega_0} \rangle$. In Eq. (36), the energy change at drive frequency $\omega_p \simeq 1\omega_0$ is

$$W_{1\omega_0} = \frac{\sqrt{\pi}}{2}(D_0\omega_0)(qE_0\Delta t) \times \exp\left[-\left(\frac{\omega_p - \omega_0}{2/\Delta t}\right)^2\right]\cos(\omega_0 t_c + \varphi_0). \quad (39)$$

The initial conditions come in by substituting D_0 and φ_0, using

$$\begin{aligned} \cos(\varphi_0) &= (x_0 - x_{1p}(0))/D_0, \\ \sin(\varphi_0) &= -(v_0 - v_{1p}(0))/D_0\omega_0, \end{aligned} \quad (40)$$

as defined in Eq. (26), and expanding $\cos(\omega_0 t_c + \varphi_0)$ to $\cos(\omega_0 t_c)\cos(\varphi_0) - \sin(\omega_0 t_c)\sin(\varphi_0)$ so that

$$D_0\cos(\omega_0 t_c + \varphi_0) = \cos(\omega_0 t_c)(x_0 - x_{1p}(0)) + \sin(\omega_0 t_c)(v_0 - v_{1p}(0))/\omega_0. \quad (41)$$

The energy change $W_{1\omega_0}$ now depends on x_0, v_0, $x_{1p}(0)$, and $v_{1p}(0)$. Similar procedure is also used to evaluate $\langle W_{2\omega_0} \rangle$ and $\langle W_{3\omega_0} \rangle$, where the sinusoidal functions are expanded and substitutions are made using Eqs. (30) and (34),

$$\begin{aligned} \cos(\phi_0) &= x_0/A_0, \\ \sin(\phi_0) &= -v_0/A_0\omega_0, \end{aligned}$$

$$\begin{aligned}\cos(\xi_0) &= -x_{2p}^{(1)}(0)/B_0,\\ \sin(\xi_0) &= v_{2p}^{(1)}(0)/B_0\omega_0,\\ \cos(\zeta_0) &= -x_{3p}^{(1)}(0)/C_0,\\ \sin(\zeta_0) &= v_{3p}^{(1)}(0)/C_0\omega_0.\end{aligned} \tag{42}$$

To compute the ensemble average of Eq. (39), the values of $\langle x_0\rangle$, $\langle v_0\rangle$, $\langle x_{1p}(0)\rangle$, and $\langle v_{1p}(0)\rangle$ are needed. The statistical moments, $\langle x_0\rangle$ and $\langle v_0\rangle$, can be evaluated given the stationary state of the harmonic oscillator in the vacuum field [2],

$$\langle x_0\rangle = 0, \quad \langle v_0\rangle = 0. \tag{43}$$

As the particular solution ($x_{1p}(0)$ and $v_{1p}(0)$) does not depend on x_0 or v_0, its ensemble average is equal to itself,

$$\begin{aligned}\langle x_{1p}(0)\rangle &= x_{1p}(0),\\ \langle v_{1p}(0)\rangle &= v_{1p}(0).\end{aligned} \tag{44}$$

The particular solutions are evaluated at $t = 0$ according to Eq. (25),

$$\begin{aligned}x_{1p}(0) &= -\int_0^\infty d\omega f_1(\omega)\sin(-\omega t_c),\\ v_{1p}(0) &= -\int_0^\infty d\omega f_1(\omega)\omega\cos(-\omega t_c),\end{aligned} \tag{45}$$

where

$$f_1(\omega) \equiv \frac{\Delta t}{2\sqrt{\pi}}\frac{qE_0}{m(\omega_0^2-\omega^2)}\exp\left[-\left(\frac{\omega-\omega_p}{2/\Delta t}\right)^2\right]. \tag{46}$$

Using the change of variables, $u \equiv \omega/\omega_0$, $u_p \equiv \omega_p/\omega_0$, $\Delta u \equiv 2/\omega_0\Delta t$, and $\kappa \equiv \omega_0 t_c$, the particular solutions in Eq. (45) can be written as

$$\begin{aligned}x_{1p}(0) &= \left(\frac{qE_0\Delta t}{m\omega_0}\frac{1}{2\sqrt{\pi}}\right)D_1,\\ v_{1p}(0) &= \left(\frac{-qE_0\Delta t}{m}\frac{1}{2\sqrt{\pi}}\right)D_2,\end{aligned} \tag{47}$$

where

$$\begin{aligned}D_1 &\equiv \int_0^\infty du\frac{1}{1-u^2}\exp\left[-\left(\frac{u-u_p}{\Delta u}\right)^2\right]\sin(\kappa u),\\ D_2 &\equiv \int_0^\infty du\frac{u}{1-u^2}\exp\left[-\left(\frac{u-u_p}{\Delta u}\right)^2\right]\cos(\kappa u).\end{aligned} \tag{48}$$

Therefore, the ensemble average of Eq. (39) is

$$\begin{aligned}\langle W_{1\omega_0}\rangle &= \frac{\sqrt{\pi}}{2}\omega_0(qE_0\Delta t)\exp\left[-\left(\frac{\omega_p-\omega_0}{2/\Delta t}\right)^2\right]\langle D_0\cos(\omega_0 t_c+\varphi_0)\rangle \\ &= \frac{-1}{4}\frac{(qE_0\Delta t)^2}{m}\exp\left[-\left(\frac{\omega_p-\omega_0}{2/\Delta t}\right)^2\right](D_1\cos(\kappa)-D_2\sin(\kappa))\,. \end{aligned} \tag{49}$$

The integral $D_1\cos(\kappa)-D_2\sin(\kappa)$ can be further evaluated,

$$\begin{aligned}&D_1\cos(\kappa)-D_2\sin(\kappa)\\ &=\int_0^\infty du\frac{1}{1-u^2}\exp\left[-\left(\frac{u-u_p}{\Delta u}\right)^2\right](\sin(\kappa u)\cos(\kappa)-u\cos(\kappa u)\sin(\kappa))\\ &=\int_0^\infty du\frac{1}{2(1+u)}\exp\left[-\left(\frac{u-u_p}{\Delta u}\right)^2\right]\sin(\kappa(u+1))\\ &\quad+\int_0^\infty du\frac{1}{2(1-u)}\exp\left[-\left(\frac{u-u_p}{\Delta u}\right)^2\right]\sin(\kappa(u-1)).\end{aligned} \tag{50}$$

Because $u_p\simeq 1$, the first term

$$\int_0^\infty du\frac{1}{2(1+u)}\exp\left[-\left(\frac{u-u_p}{\Delta u}\right)^2\right]\sin(\kappa(u+1)) \tag{51}$$

is effectively zero. Let $u_p=1-\epsilon\Delta u$, where $\epsilon\ll 1$ is a small number, we obtain

$$D_1\cos(\kappa)-D_2\sin(\kappa)=\frac{-1}{2}\int_0^\infty du\frac{\sin(\kappa(u-1))}{u-1}\exp\left[-\left(\frac{u-1}{\Delta u}+\epsilon\right)^2\right]. \tag{52}$$

By the change of variables $x\equiv(u-1)/\Delta u$ and $\alpha\equiv\kappa\Delta u$, the above integral can be rewritten as

$$\int_0^\infty du\frac{\sin(\kappa(u-1))}{u-1}\exp\left[-\left(\frac{u-1}{\Delta u}+\epsilon\right)^2\right]=\int_{-1/\Delta u}^\infty dx\frac{\sin(\alpha x)}{x}\exp\left[-(x+\epsilon)^2\right]. \tag{53}$$

Because the width of the integrand is much smaller than the lower integral limit, $\pi/\alpha\ll 1/\Delta u$, the integral can be approximated by extending the lower limit to the negative infinity,

$$\int_{-1/\Delta u}^\infty dx\frac{\sin(\alpha x)}{x}\exp\left[-(x+\epsilon)^2\right]\simeq\int_{-\infty}^{+\infty}dx\frac{\sin(\alpha x)}{x}\exp\left[-(x+\epsilon)^2\right], \tag{54}$$

which can be written in the complex form,

$$\int_{-\infty}^{+\infty} dx \frac{\sin(\alpha x)}{x} \exp\left[-(x+\epsilon)^2\right] = \mathrm{Im}\left(\int_{-\infty}^{+\infty} dx \frac{e^{i\alpha x}}{x} \exp\left[-(x+\epsilon)^2\right]\right). \quad (55)$$

We will use the contour integral to evaluate this complex integral,

$$\begin{aligned}\oint_C dz \frac{e^{i\alpha z}}{z} \exp\left[-|z+\epsilon|^2\right] &= \int_{C_S} dz \frac{e^{i\alpha z}}{z} \exp\left[-|z+\epsilon|^2\right] \\ &+ \int_{C_L} dz \frac{e^{i\alpha z}}{z} \exp\left[-|z+\epsilon|^2\right] \\ &+ \int_{-\infty}^{+\infty} dx \frac{e^{i\alpha x}}{x} \exp\left[-(x+\epsilon)^2\right]. \end{aligned} \quad (56)$$

The contour C consists of one large hemicircles C_L on the upper-half of the complex plane, one small hemicircle C_S on the lower-half complex plane around the pole $z = 0$, and a line on the real axis from the negative infinity to the positive infinity. The integral along C_L is zero according to Jordan's lemma,

$$\int_{C_L} dz \frac{e^{i\alpha z}}{z} \exp\left[-|z+\epsilon|^2\right] = 0. \quad (57)$$

The integral along C_S can be evaluated as

$$\int_{C_S} dz \frac{e^{i\alpha z}}{z} \exp\left[-|z+\epsilon|^2\right] = \pi i \left(e^{i\alpha z} \exp\left[-|z+\epsilon|^2\right]\right)\Big|_{z=0} = \pi i e^{-\epsilon^2}. \quad (58)$$

The contour integral is evaluated accordingly to the Cauchy integral formula,

$$\oint_C dz \frac{e^{i\alpha z}}{z} \exp\left[-|z+\epsilon|^2\right] = 2\pi i \left(e^{i\alpha z} \exp\left[-|z+\epsilon|^2\right]\right)\Big|_{z=0} = 2\pi i e^{-\epsilon^2}. \quad (59)$$

Therefore, we obtain for values of $\alpha \gg 1$ the value of the integral in Eq. (55),

$$\int_{-\infty}^{+\infty} dx \frac{\sin(\alpha x)}{x} \exp\left[-(x+\epsilon)^2\right] = \mathrm{Im}\left(\pi i e^{-\epsilon^2}\right) = \pi e^{-\epsilon^2}. \quad (60)$$

Combining Eqs. (52), (53), (54), and (55), the integral $D_1 \cos(\kappa) - D_2 \sin(\kappa)$ in Eq. (49) can be evaluated,

$$D_1 \cos(\kappa) - D_2 \sin(\kappa) = \frac{-\pi}{2} \exp\left[-\left(\frac{\omega_p - \omega_0}{2/\Delta t}\right)^2\right]. \quad (61)$$

Given Eqs. (49) and (61), the ensemble average of the energy change at drive frequency $\omega_p \simeq 1\omega_0$ is

$$\langle W_{1\omega_0}\rangle = \frac{\pi}{8}\frac{(qE_0\Delta t)^2}{m}\exp\left[-2\left(\frac{\omega_p-\omega_0}{2/\Delta t}\right)^2\right]. \tag{62}$$

7 Quantum Perturbation Analysis

In this appendix, we use the second-order quantum perturbation to obtain the energy expectation value for an harmonic oscillator that is excited by a propagating Gaussian pulse. The Gaussian pulse is calculated beyond dipole approximation. In other words, the pulse field has spatial dependence in addition to its temporal dependence. The agreement between quantum perturbation analysis and quantum simulation is about 80 %. The result of the quantum analysis is similar to that of the classical analysis given in Eq. (37). A brief summary for the derivation of the quantum analysis is given in the following. The quantum state of an harmonic oscillator is

$$|\psi\rangle(t) = \sum_{n=0}^{\infty} c_n(t)e^{-i\omega_n t}|n\rangle, \tag{63}$$

where $|n\rangle$ is the unperturbed eigenstate, $\omega_n = \omega_0(n+1/2)$ is the eigenfrequency, and $c_n(t)$ is the probability amplitude. In the interaction picture, the Schrödinger equation with the unperturbed Hamiltonian $\widehat{H}_0$ and the perturbative Hamiltonian $\widehat{H}'$ can be generally written as

$$i\hbar\frac{d}{dt}\left(\sum_{n=0}^{\infty} c_n(t)|n\rangle\right) = \widehat{\mathscr{H}}\left(\sum_{n=0}^{\infty} c_m(t)|m\rangle\right), \tag{64}$$

where $\widehat{\mathscr{H}} = e^{\frac{i}{\hbar}\widehat{H}_0 t}\widehat{H}' e^{-\frac{i}{\hbar}\widehat{H}_0 t}$. Using the second-order perturbation theory, the perturbative expansion of the probability amplitude $c_n(t) \simeq c_n^{(0)}(t) + \lambda_n c_n^{(1)}(t) + \lambda_n^2 c_n^{(2)}(t)$ turns the Schrödinger equation into a system of equations,

$$\begin{cases} i\hbar\frac{d}{dt}\left(\sum_{n=0}^{\infty} c_n^{(0)}(t)|n\rangle\right) & = 0 \\ i\hbar\frac{d}{dt}\left(\sum_{n=0}^{\infty} \lambda_n c_n^{(1)}(t)|n\rangle\right) & = \widehat{H}'\left(\sum_{n=0}^{\infty} c_m^{(0)}(t)|m\rangle\right) \\ i\hbar\frac{d}{dt}\left(\sum_{n=0}^{\infty} \lambda_n^2 c_n^{(2)}(t)|n\rangle\right) & = \widehat{H}'\left(\sum_{n=0}^{\infty} \lambda_n c_m^{(1)}(t)|m\rangle\right), \end{cases} \tag{65}$$

where λ_n denotes the expansion factor for $c_n(t)$. In our study, the perturbative Hamiltonian $\widehat{H}'$ is provided by the interaction between a charged quantum particle and a classical field,

$$\widehat{H}' = -\frac{q}{2m}\left(2\mathbf{A}_p\cdot\hat{\mathbf{p}} - q\mathbf{A}_p^2\right), \tag{66}$$

where q and m are the charge and the mass of the particle. The driving field $\mathbf{A}_p$ is a propagating Gaussian pulse,

$$\mathbf{A}_p = A_p \cos\left(\mathbf{k}_p \cdot \hat{\mathbf{x}} - \omega_p \tau\right) \exp\left[-\left(\frac{\mathbf{k}_p \cdot \hat{\mathbf{x}}}{|\mathbf{k}_p|\Delta x} - \frac{\tau}{\Delta t}\right)^2\right] \boldsymbol{\varepsilon}_p, \tag{67}$$

where $\tau = t - t_c$, $\mathbf{k}_p = \omega_p/c\left(\sin\theta_p, 0, \cos\theta_p\right)$ is the wave vector of the field and $\boldsymbol{\varepsilon}_p = \left(\cos\theta_p, 0, -\sin\theta_p\right)$ is the field polarization. Note that in order to take the calculation beyond the dipole approximation, we will keep the operator $\hat{\mathbf{x}}$ in the function form of the driving field $\mathbf{A}_p$. Using $\mathbf{k}_p \cdot \hat{\mathbf{x}}$ as an expansion factor for $\mathbf{A}_p$, the perturbative Hamiltonian can be expanded. In the interaction picture, the expanded perturbative Hamiltonian is

$$\widehat{\mathscr{H}} \simeq \widehat{\mathscr{H}_{1\omega_0}}(t) + \widehat{\mathscr{H}_{2\omega_0}}(t) + \widehat{\mathscr{H}_{3\omega_0}}(t), \tag{68}$$

where

$$\begin{aligned}
\widehat{\mathscr{H}_{1\omega_0}}(t) &= f_1(t)\left(\hat{b}^\dagger e^{i\omega_0 t} - \hat{b}e^{-i\omega_0 t}\right), \\
\widehat{\mathscr{H}_{2\omega_0}}(t) &= f_2(t)\left(\hat{b}^{\dagger 2} e^{i2\omega_0 t} + \hat{\mathbb{1}} - \hat{b}^2 e^{-i2\omega_0 t}\right), \\
\widehat{\mathscr{H}_{3\omega_0}}(t) &= f_3(t)\left[\hat{b}^{\dagger 3} e^{i3\omega_0 t} + \left(\hat{b}\hat{b}^{\dagger 2} e^{i\omega_0 t} - \hat{b}^\dagger \hat{b}^2 e^{-i\omega_0 t}\right)\right. \\
&\quad \left. + \left(\hat{b}^\dagger e^{i\omega_0 t} + \hat{b}e^{-i\omega_0 t}\right) - \hat{b}^3 e^{-i3\omega_0 t}\right] + g_3(t)\hat{\mathbb{1}}.
\end{aligned} \tag{69}$$

The symbol $\hat{b}^\dagger$ and $\hat{b}$ are the raising and the lowing operators for the harmonic oscillator. The symbol $\hat{\mathbb{1}}$ denotes the identity operator.

The time-dependent functions $f_1(t)$, $f_2(t)$, $f_3(t)$, and $g_3(t)$ are defined as

$$\begin{aligned}
f_1(t) &= \left[\left(\frac{-qA_p\varepsilon_x}{m}\right) i\sqrt{\frac{\hbar m\omega_0}{2}}\right] \cos\left(\omega_p\tau\right) \exp\left(-\tau^2/\Delta t^2\right), \\
f_2(t) &= \left[\left(\frac{-qA_p\varepsilon_x}{m}\right) k_x \sqrt{\frac{\hbar}{2m\omega_0}} i\sqrt{\frac{\hbar m\omega_0}{2}}\right] \sin\left(\omega_p\tau\right) \exp\left(-\tau^2/\Delta t^2\right), \\
f_3(t) &= \left[\left(\frac{qA_p\varepsilon_x}{m}\right) \frac{k_x^2}{2}\left(\sqrt{\frac{\hbar}{2m\omega_0}}\right)^2 i\sqrt{\frac{\hbar m\omega_0}{2}}\right] \cos\left(\omega_p\tau\right) \exp\left(-\tau^2/\Delta t^2\right), \\
g_3(t) &= \left(\frac{-q^2A_p^2}{m}\right) \cos^2\left(\omega_p\tau\right) \exp\left(-\tau^2/\Delta t^2\right).
\end{aligned} \tag{70}$$

In the case of $1\omega_0$-excitation with $\omega_p \simeq 1\omega_0$, only the $\widehat{\mathscr{H}_{1\omega_0}}(t)$ term is effective. In the cases of $2\omega_0$-excitation with $\omega_p \simeq 2\omega_0$, only the $\widehat{\mathscr{H}_{2\omega_0}}(t)$ term is effective. In the case of $3\omega_0$-excitation with $\omega_p \simeq 3\omega_0$, only the $\widehat{\mathscr{H}_{3\omega_0}}(t)$ term is effective. Assuming

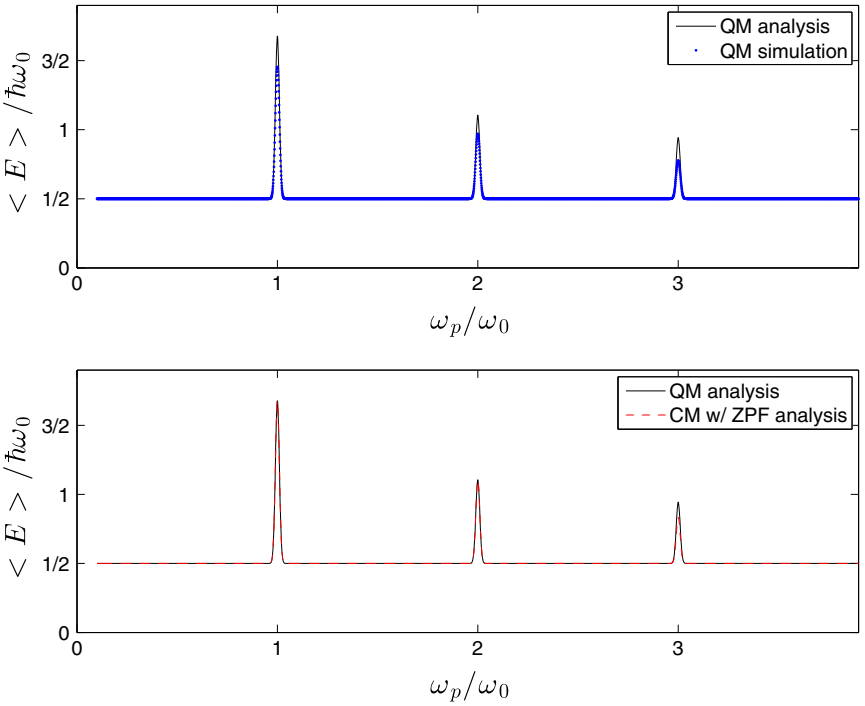

Fig. 3 Comparison between quantum analysis, quantum simulation, and classical analysis. *Up* the overall agreement between quantum perturbation and quantum simulation is within 80 %. *Bottom* the quantum analysis and the classical analysis shows identical resonance structures at $\omega_p \simeq 1\omega_0$ and $\omega_p \simeq 2\omega_0$, while the agreement at $\omega_p \simeq 3\omega_0$ is about 65 %

that the harmonic oscillator is initially at the ground state, the expectation value of the energy change can be calculated up to λ_n^2,

$$\begin{aligned}
\langle \Delta E_{1\omega_0} \rangle &= \frac{\pi}{8}\left(\frac{q^2 A_p^2 \omega_0^2 \Delta t^2}{m}\right) \exp\left[-2\left(\frac{\omega_p - \omega_0}{2/\Delta t}\right)^2\right] \cos^2(\theta_p), \\
\langle \Delta E_{2\omega_0} \rangle &= \frac{\pi}{16}\left(\frac{4q^2 A_p^2 \omega_0^2 \Delta t^2}{m}\right)\left(\frac{\hbar\omega_p}{mc^2}\right)\left(\frac{\omega_p}{\omega_0}\right) \sin^2(\theta_p) \\
&\quad \times \exp\left[-2\left(\frac{\omega_p - 2\omega_0}{2/\Delta t}\right)^2\right] \cos^2(\theta_p), \\
\langle \Delta E_{3\omega_0} \rangle &= \frac{3\pi}{16^2}\left(\frac{12q^2 A_p^2 \omega_0^2 \Delta t^2}{m}\right)\left[\left(\frac{\hbar\omega_p}{mc^2}\right)\left(\frac{\omega_p}{\omega_0}\right) \sin^2(\theta_p)\right]^2 \\
&\quad \times \exp\left[-2\left(\frac{\omega_p - 3\omega_0}{2/\Delta t}\right)^2\right] \cos^2(\theta_p). \qquad (71)
\end{aligned}$$

The result of quantum perturbation analysis, Eq. (71), is compared with quantum simulation in Fig. 3. The agreement is about 80 %. In the same figure, the quantum

analysis is also compared with the classical analysis, Eq. (37). The quantum analysis agrees well with the classical analysis, as evidenced by the similarity between Eqs. (71) and (37).

References

1. Boyer, T.H.: Random electrodynamics: the theory of classical electrodynamics with classical electromagnetic zero-point radiation. Phys. Rev. D **11**, 790 (1975)
2. Boyer, T.H.: General connection between random electrodynamics and quantum electrodynamics for free electromagnetic fields and for dipole oscillator systems. Phys. Rev. D **11**, 809 (1975)
3. Milonni, P.W.: The Quantum Vacuum: An Introduction to Quantum Electrodynamics. Academic Press, Boston (1994)
4. Cetto, A.M., de la Peña, L., Valdés-Hernández, A.: Quantization as an emergent phenomenon due to matter-zeropoint field interaction. J. Phys. **361**, 012013 (2012)
5. Cetto, A.M., de la Peña, L.: The Quantum Dice, an Introduction to Stochastic Electrodynamics. Kluwer, Dordrecht (1996)
6. Boyer, T.H.: Asymptotic retarded van der Waals forces derived from classical electrodynamics with classical electromagnetic zero-point radiation. Phys. Rev. A **5**, 1799 (1972)
7. Dressel, J., Bliokh, K.Y., Nori, F.: Classical field approach to quantum weak measurements. Phys. Rev. Lett. **112**, 110407 (2014)
8. Milonni, P.W.: The Quantum Vacuum: An Introduction to Quantum Electrodynamics. Academic Press, Boston (1994)
9. P. W. Milonni, The Quantum Vacuum: An Introduction to Quantum Electrodynamics, pp. 51–54, 123–128, 487–488. Academic Press, Boston (1994)
10. Griffiths, D.J.: Introduction to Electrodynamics, 3rd edn. Prentice-Hall, Upper Saddle River (1999)
11. Landau, L.D., Lifshitz, E.M.: The Classical Theory of Fields, 4th edn, p. 207. Pergamon Press, New York (1987). (Eq. 75.10)
12. Jackson, J.D.: Classical Electrodynamics, 3rd edn, p. 749. Wiley, New York (1998). (Eq. 16.10)
13. Huang, W., Batelaan, H.: Dynamics underlying the Gaussian distribution of the classical harmonic oscillator in zero-point radiation. J. Comput. Methods Phys. **2013**, 308538 (2013)
14. Thornton, S.T., Marion, J.B.: Classical Dynamics of Particles and Systems, 5th edn, pp. 117–128. Brooks/Cole, Belmont (2004)
15. Landau, L.D., Lifshitz, E.M.: Mechanics, 3rd edn, p. 80. Butterworth-Heinemann, Oxford (1976)
16. Yariv, A.: Quantum Electronics, 3rd edn, p. 407. Wiley, New York (1988)
17. Heisenberg, W.: Über quantentheoretische Umdeutung kinematischer und mechanischer Besiehungen. Z. Phys. **33**, 879 (1925)
18. Aitchison, I.J.R., MacManus, D.A., Snyder, T.M.: Understanding Heisenbergs magical paper of July 1925: a new look at the calculational details. Am. J. Phys. **72**, 11 (2004)
19. Averbukh, V., Moiseyev, N.: Classical versus quantum harmonic-generation spectrum of a driven anharmonic oscillator in the high-frequency regime. Phys. Rev. A **57**, 1345 (1998)
20. Griffiths, D.J.: Introduction to Quantum Mechanics, 2nd edn, p. 366. Upper Saddle River, Pearson Prentice Hall (2005)